IFASD 2015
International Forum on Aeroelasticity and Structural Dynamics
June 28 — July 02, 2015 ▲ Saint Petersburg, Russia

# Asymmetric limit cycle oscillations in systems with symmetric freeplay

Grigorios Dimitriadis

Aerospace and Mechanical Engineering Department

Quartier Polytech 1, Allée de la Découverte 9, 4000, Liège, Belgium

**Keywords:** Nonlinear aeroelasticity, Freeplay, Limit Cycle Oscillations, Bifurcation.

**Abstract:** In this paper, a simple 2D aeroelastic system with degrees of freedom in pitch, plunge and control surface deflection is investigated with freeplay in the pitch degree of freedom. It is shown that this system features a fixed point at the origin as well as two anti-symmetric fixed points. Asymmetric limit cycles that span only two of the three piecewise linear subdomains of the phase plane can orbit these anti-symmetric fixed points. A single three-domain symmetric cycle and two two-domain cycles appear as a result of a grazing bifurcation occurring at the flutter speed of the underlying linear system. The two-domain cycles can undergo further fold, period doubling and torus bifurcations. They can cause both periodic and aperiodic oscillations, including highly chaotic responses at parameter values where they interact strongly.

## 1 INTRODUCTION

Freeplay in actuators and bearings is a significant source of nonlinearity in aeroelastic systems. Airworthiness authorities place very strict limits on the amount of freeplay allowed in aircraft control surfaces (see [1] for example). Assessing the impact of freeplay on aeroelastic responses is therefore an important aspect of nonlinear aeroelastic research.

Several authors have investigated the aeroelastic behavior of simple systems with freeplay, paying particular attention to Limit Cycle Oscillation (LCO) phenomena [2, 3, 4, 5]. Conner et al [3] in particular analysed a rectangular wing with pitch, plunge and control degrees of freedom and freeplay in the control spring, both theoretically and experimentally. The system was shown to undergo several different type of LCO, including asymmetric and aperiodic oscillations. The asymmetric LCOs occur as a result of a symmetry-breaking bifurcation caused by the interaction between two independent limit cycle branches. These branches are created by different bifurcation events. Nevertheless, all the LCOs orbit the single fixed point lying at the origin.

In this paper, the same system is investigated but with freeplay in the pitch degree of freedom instead of the control. It is shown that the position of the freeplay can cause new anti-symmetric fixed points to come into existence and that limit cycles can orbits these new fixed points. This phenomenon is interesting because the system is completely symmetric and yet gives rise to asymmetric periodic responses and fixed points. The paper attempts to explain this phenomenon using equivalent linearisation.

## 2 MATHEMATICAL MODEL

The pitch-plunge-control aeroelastic system is a 2D symmetric flat plate wing with a control surface. The entire wing is suspended by an extension spring with stiffness $K_h$ and a rotational spring of stiffness $K_\alpha$ from its flexural axis $x_f$. These two springs provide restoring forces in the plunge, $h$, and pitch, $\alpha$, degrees of freedom respectively. The control surface deflection angle $\beta$ is an additional degree of freedom, restrained by a rotational spring with stiffness $K_\beta$. The control surface hinge lies at $x_h$ and the total chord of the wing is denoted by $c$. The complete system is plotted in figure 1.

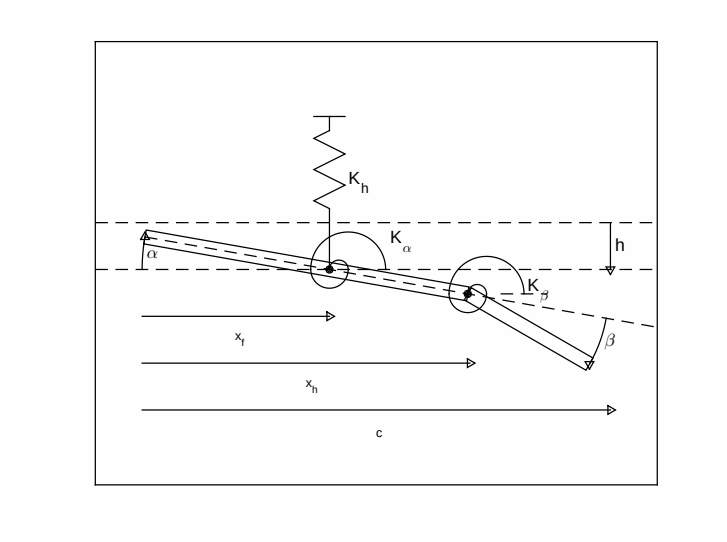


Figure 1: Pitch-plunge-control aeroelastic system

It is now assumed that there is freeplay in the pitch degree of freedom, such that the spring restoring force in the pitch degree of freedom is zero while $|\alpha| < \delta$, $2\delta$ being the width of the freeplay region. Figure 2 shows a typical restoring force diagram for freeplay, whereby the stiffness is $K$ is $|\alpha| > \delta$ and zero otherwise. Note that the freeplay region is centred around the origin.

In the case of the pitch-plunge-control wing with freeplay in the pitch degree of freedom, the stiffness outside the freeplay region is given by $K_\alpha$, while the stiffness inside the freeplay region is zero as usual. The restoring moment equation is given by

$$M_\alpha(\alpha) = \begin{cases} K_\alpha(\alpha + \delta) & \text{if} \quad \alpha < -\delta \\ 0 & \text{if} \quad |\alpha| \leq \delta \\ K_\alpha(\alpha - \delta) & \text{if} \quad \alpha > \delta \end{cases} \tag{1}$$

where $M_\alpha$ is the pitching moment provided by the freeplay spring.

The equations of motion of the system flying with airspeed $U$ in air of density $\rho$ can be developed using linear unsteady attached flow aerodynamic assumptions; a time-domain model can be developed by means of Wagner function analysis [3, 5]. The structural displacements are denoted by the vector $\mathbf{y} = [h \quad \alpha \quad \beta]$ while the 6 aerodynamic states are denoted by the vector $\mathbf{w} = [w_1 \quad \dots \quad w_6]$. Then the complete state vector of the system is given by $\mathbf{x} = [\dot{\mathbf{y}} \quad \mathbf{y} \quad \mathbf{w}]^T$ and has dimensions $12 \times 1$. The equations of motion

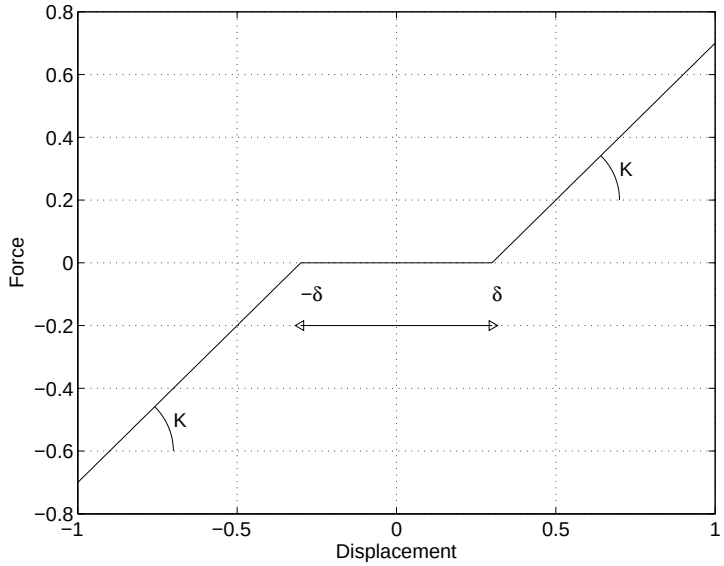


Figure 2: Freeplay stiffness diagram

of the system with freeplay in the control surface are given by

$$\dot{\mathbf{x}} = \mathbf{Q}_1\mathbf{x} + \mathbf{q}_n M_\alpha(\alpha) \tag{2}$$

where

$$\begin{aligned} \mathbf{Q}_1 &= \begin{pmatrix} -\mathbf{M}^{-1}(\mathbf{C}+\rho U\mathbf{D}) & -\mathbf{M}^{-1}(\mathbf{E}_1+\rho U^2\mathbf{F}) & -\rho U^3\mathbf{M}^{-1}\mathbf{W} \\ \mathbf{I}_{3\times3} & \mathbf{0}_{3\times3} & \mathbf{0}_{3\times6} \\ \mathbf{0}_{6\times3} & \mathbf{W}_1 & U\mathbf{W}_2 \end{pmatrix} \\ \mathbf{q}_n &= \begin{pmatrix} -\mathbf{M}^{-1}\begin{pmatrix} 0 \\ 1 \\ 0 \end{pmatrix} \\ \mathbf{0}_{9\times1} \end{pmatrix} \end{aligned} \tag{3}$$

and $\mathbf{E}_1$, is the value of the structural stiffness matrix inside the freeplay region $\pm\delta$, given by

$$\mathbf{E}_1 = \begin{pmatrix} K_h & 0 & 0 \\ 0 & 0 & 0 \\ 0 & 0 & K_\beta \end{pmatrix} \tag{4}$$

Matrix $\mathbf{C}$ is the structural damping matrix, $\rho U\mathbf{D}$ is the aerodynamic damping matrix, $\rho U^2\mathbf{F}$ is the aerodynamic stiffness matrix, $\mathbf{W}$ is the aerodynamic state matrix, $\mathbf{W}_1$ and $\mathbf{W}_2$ are the aerodynamic state equation matrices, $\mathbf{M} = \mathbf{A} + \rho\mathbf{B}$, $\mathbf{A}$ is the structural mass matrix and $\mathbf{B}$ is the aerodynamic mass matrix. The notation $\mathbf{I}_{3\times3}$ denotes a unit matrix of size $3 \times 3$. The values of all the matrices are given in the appendix. Equations 2 can be written as

$$\dot{\mathbf{x}} = \mathbf{Q}_1\mathbf{x} \quad \text{if} \quad |\alpha| \le \delta \tag{5}$$

$$\dot{\mathbf{x}} = \mathbf{Q}_2\mathbf{x} - \mathbf{q}_n K_\alpha \operatorname{sgn}(\alpha)\delta \quad \text{if} \quad |\alpha| > \delta \tag{6}$$

where $\mathbf{Q}_2\mathbf{x} = \mathbf{Q}_1\mathbf{x} + \mathbf{q}_n K_\alpha \alpha$. Note that

$$\dot{\mathbf{x}} = \mathbf{Q}_2\mathbf{x}$$

is the equation of motion of the nominal system with full stiffness. This system will be referred to as the overlying linear system. The system of equation 5 will be referred to as the underlying linear system.

## 3 SYSTEM FIXED POINTS

The freeplay function of figure 1 splits the phase plane of the system responses into three piecewise linear subdomains, $S_1$ for $|\alpha| \leq \delta$, $S_2$ for $\alpha > \delta$ and $S_3$ for $\alpha < -\delta$. Response trajectories can span one, two or all three of the subdomains. Furthermore, equation 2 has three fixed points given by

$$\begin{aligned} \mathbf{x}_{F_1} &= \mathbf{0} \quad \text{if} \quad |\alpha| \leq \delta \\ \mathbf{x}_{F_2} &= \mathbf{Q}_2^{-1}\mathbf{q}_n K_\alpha \delta \quad \text{if} \quad \alpha > \delta \\ \mathbf{x}_{F_3} &= -\mathbf{Q}_2^{-1}\mathbf{q}_n K_\alpha \delta \quad \text{if} \quad \alpha < -\delta \end{aligned} \tag{7}$$

These fixed points do not coexist; only one of them is an attractor at any instance in time, depending on which subdomain the response trajectory lies in. Note that $\mathbf{x}_{F_1}$ always lies in $S_1$, $\mathbf{x}_{F_2}$ can lie in $S_1$ or $S_2$ and $\mathbf{x}_{F_3}$ can lie in $S_1$ or $S_3$. If points $\mathbf{x}_{F_{2,3}}$ lie in $S_1$ they cannot exist, since they are fixed points of equation 6 which is not defined in $S_1$. Therefore, the condition for their existence is

$$|\alpha_{F_{2,3}}| > \delta$$

where $\alpha_{F_{2,3}}$ is the pitch component of these two fixed points. It can be shown that the condition is only a function of the overlying linear system and the position of the nonlinearity.

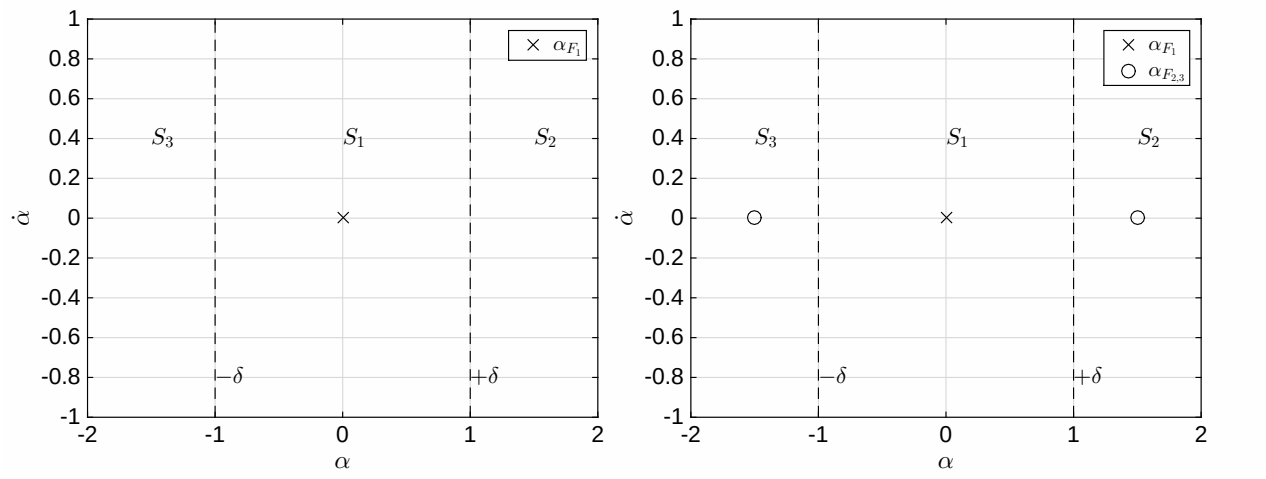


(a) Case 1 (b) Case 2

Figure 3: Two possible fixed point cases.

There are two cases for the fixed points of equations 2, demonstrated graphically in figure 3, which plots the positions of the fixed points in the $\alpha - \dot{\alpha}$ phase plane. The plot of subfigure 3(a) shows the case where $|\alpha_{F_{2,3}}| < \delta$ and therefore only $\mathbf{x}_{F_1}$ exists. Subfigure 3(b) demonstrates the case where $|\alpha_{F_{2,3}}| > \delta$ and all three fixed points exist.

## 4 TWO-DOMAIN AND THREE-DOMAIN LIMIT CYCLES

It is reasonable to make the assumption that the overlying (i.e. nominal) linear system is flutter-free and divergence-free and that any aeroelastic instabilities are due to the freeplay. Furthermore, it will be assumed that the flutter speed of the underlying linear system $U_{F_1}$ is lower than that of the overlying linear system, $U_{F_2}$. Two types of periodic solution are then possible:

- Circles: These exist entirely in the $S_1$ subdomain and can only occur at the flutter point of the underlying linear system, i.e. when $U = U_{F_1}$.
- Limit cycles: These must span at least two subdomains as they can only exist if the system is nonlinear. They can exist at a range of airspeeds.

The circles and limit cycles are related; the circles bifurcate into limit cycles when their amplitude becomes equal to the width of the freeplay boundary. This bifurcation is known as a grazing bifurcation (see for example [6]). Limit cycles that span two domains, i.e. $S_1$ and $S_2$ or $S_1$ and $S_3$ are referred to as two-domain cycles. Limit cycles that span all three domains are referred to as three-domain cycles. Figure 4 plots both types of limit cycle. It can be seen that a three-domain cycle will orbit $\mathbf{x}_1$ and $\mathbf{x}_{2,3}$ if they exist. In contrast, a two-domain cycle can only orbit either $\mathbf{x}_2$ or $\mathbf{x}_3$. It follows that two-domain cycles can only exist if the fixed points $\mathbf{x}_{2,3}$ also exist.

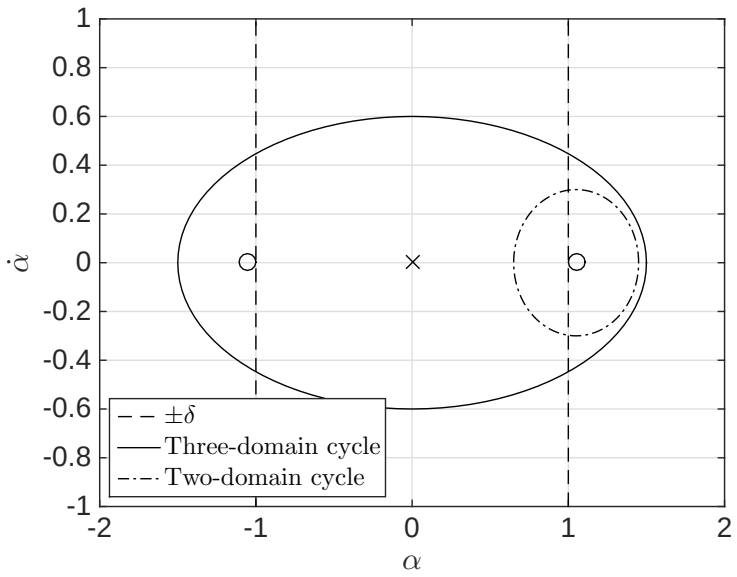


Figure 4: Two-domain and three-domain cycles

Limit cycles can be easily approximated using the equivalent linearization (or describing function) approach. The periodic pitch response is approximated by a sinusoidal function of time

$$\alpha(t) = A \sin \omega t + \alpha_0$$

Three-domain cycles orbit $\mathbf{x}_1 = \mathbf{0}$ and are therefore characterized by $\alpha_0 = 0$. For two-domain cycles, $\alpha_0 \neq 0$. The nonlinear restoring moment of equation 1 is approximated as

a Fourier series of the form

$$M_\alpha(\alpha) = a_0 + a_1 \cos\omega t + b_1 \sin\omega t$$

where

$$\begin{aligned} a_0 &= \frac{\omega}{2\pi}\int_{-\pi/\omega}^{\pi/\omega} M(A\sin\omega t + \alpha_0)dt \\ a_1 &= \frac{\omega}{\pi}\int_{-\pi/\omega}^{\pi/\omega} M(A\sin\omega t + \alpha_0)\cos\omega t dt \\ b_1 &= \frac{\omega}{\pi}\int_{-\pi/\omega}^{\pi/\omega} M(A\sin\omega t + \alpha_0)\sin\omega t dt \end{aligned} \tag{8}$$

Carrying out the integrations for a three-domain cycle, we obtain $a_0 = 0$, $a_1 = 0$ and

$$b_1 = AK_\alpha - A\frac{K_\alpha}{\pi}(2\sigma + \sin 2\sigma)$$

where

$$\sigma = \sin^{-1}\frac{\delta}{A} \tag{9}$$

The ratio $b_1/A$ is known as the equivalent linear stiffness, given by

$$K_{eq}(A) = K_\alpha - \frac{K_\alpha}{\pi}(2\sigma + \sin 2\sigma) \tag{10}$$

The condition for periodic solutions with amplitude $A$ to exist is that $\sigma$ must be real, i.e. $A > \delta$. This result is consistent with the definition of a three-domain limit cycle, since $A\sin\omega t$ will span all three piecewise linear subdomains.

A relationship between limit cycle amplitude $A$ and airspeed $U$ can be obtained by calculating the flutter speed of the equivalent linear system

$$\dot{\mathbf{x}} = \mathbf{Q}_{eq}\mathbf{x} \tag{11}$$

where $\mathbf{Q}_{eq}\mathbf{x} = \mathbf{Q}_1\mathbf{x} + \mathbf{q}_n K_{eq}(A)\alpha$ for different values of $A$. For $A = \delta$, i.e. the minimum possible limit cycle amplitude, $K_eq = 0$ and the equivalent linear system becomes the underlying linear system. This means that three-domain limit cycles appear at the flutter speed of the underlying linear system, $U_{F_1}$. Note also that

$$\lim_{A\to\infty} K_{eq}(A) = K_\alpha$$

i.e. the limit cycle amplitude tends to infinity when the equivalent linear system becomes the overlying linear system. In other words, the nonlinear system with freeplay becomes completely unstable at the flutter airspeed of the nominal linear system, $U_{F_2}$.

[7, 8] and others developed equivalent stiffness expressions for freeplay with and without preload, such as the one presented in equation 10. In all these works, the resulting periodic solutions are centered around the fixed point $\mathbf{x}_1$. In this paper, the emphasis is

on identifying periodic solutions that are not centred around $\mathbf{x}_1$. For a two-domain limit cycle the integrals of equations 8 yield

$$\begin{aligned} a_0 &= \frac{K_\alpha \alpha_0}{2} - \frac{K_\alpha \delta}{2} + \frac{AK_\alpha}{\pi}\left(\sigma_1 \sin\sigma_1 + \cos\sigma_1\right) \\ a_1 &= 0 \\ b_1 &= A\frac{K_\alpha}{2} - A\frac{K_\alpha}{2\pi}\left(2\sigma_1 + \sin 2\sigma_1\right) \end{aligned} \tag{12}$$

where

$$\sigma_1 = \sin^{-1}\frac{\delta - \alpha_0}{A} \tag{13}$$

and the equivalent linear stiffness is given by

$$K_{eq}(A) = \frac{K_\alpha}{2} - \frac{K_\alpha}{2\pi}\left(2\sigma_1 + \sin 2\sigma_1\right) \tag{14}$$

The condition for existence of such limit cycles is that $\sigma_1$ is real, i.e. $A > |\delta - \alpha_0|$. This means that neither the upper nor the lower bound of the cycle can cross a freeplay boundary. For example, a two-domain cycle spanning $S_1$ and $S_2$ will disappear if either of the two bounds cross $+\delta$. Note that $\sigma_1$ takes values between $-\pi/2 \leq \sigma_1 \leq \pi/2$, while $\delta - \alpha_0$ spans $-A \leq \delta - \alpha_0 \leq A$.

For the right limit $\sigma_1 = \pi/2$, $\delta - \alpha_0 = A$, substituting into equations 12 and 14 yields

$$a_0 = 0, \quad K_{eq} = 0,$$

while for the left limit $\sigma_1 = -\pi/2$, $\delta - \alpha_0 = -A$ we obtain

$$a_0 = K_\alpha(\alpha_0 + \delta), \quad K_{eq} = K_\alpha$$

In other words, two-domain limit cycles appear when the equivalent stiffness is equal to the stiffness of the underlying linear system and disappear when $K_{eq}$ is equal to the stiffness of the overlying linear system. A relationship between limit cycle amplitude $A$, centre $\alpha_0$ and airspeed $U$ can be obtained by calculating the flutter speed of the equivalent linear system

$$\dot{\mathbf{x}} = \mathbf{Q}_{eq}\mathbf{x} + \mathbf{q}_n a_0 \tag{15}$$

for different values of $A$ and $\alpha_0$, where $\mathbf{Q}_{eq}\mathbf{x} = \mathbf{Q}_1\mathbf{x} + \mathbf{q}_n K_{eq}(A)\alpha$ and $K_eq$ is calculated from equation 14. Note that this equivalent linear system has a fixed point lying at

$$\mathbf{x}_{F_{eq}} = -\mathbf{Q}_{eq}^{-1}\mathbf{q}_n a_0$$

The equivalent linear solution process is more complex for two-domain cycles than for three-domain cycles. Each point on a limit cycle branch is characterized by a particular value for $A$, $U$ and $\alpha_0$. A convenient solution scheme is to choose a value for $K_{eq}$ between 0 and $K_\alpha$ and then calculate the flutter speed of the resulting equivalent linear system. It remains to find values of $A$ and $\alpha_0$ that will yield the correct $K_eq$ and $\alpha_{F_{eq}}$, where $\alpha_{F_{eq}}$ is the pitch component of $\mathbf{x}_{F_{eq}}$. The nonlinear algebraic system

$$\begin{aligned} K_{eq} - \frac{K_\alpha}{2} - \frac{K_\alpha}{2\pi}\left(2\sigma_1 + \sin 2\sigma_1\right) &= 0 \\ \alpha_{F_{eq}} - \alpha_0 &= 0 \end{aligned} \tag{16}$$

can be set up and solved using Newton iterations. The starting point of the limit cycle branch is $K_{eq} = 0$, $U = U_{F_1}$, $a_0 = 0$, for which the only possible limit cycle is a circle with amplitude $A = \delta$ and $\alpha_0 = 0$. The final point on the branch is $K_{eq} = K_\alpha$, $U = U_{F_2}$.

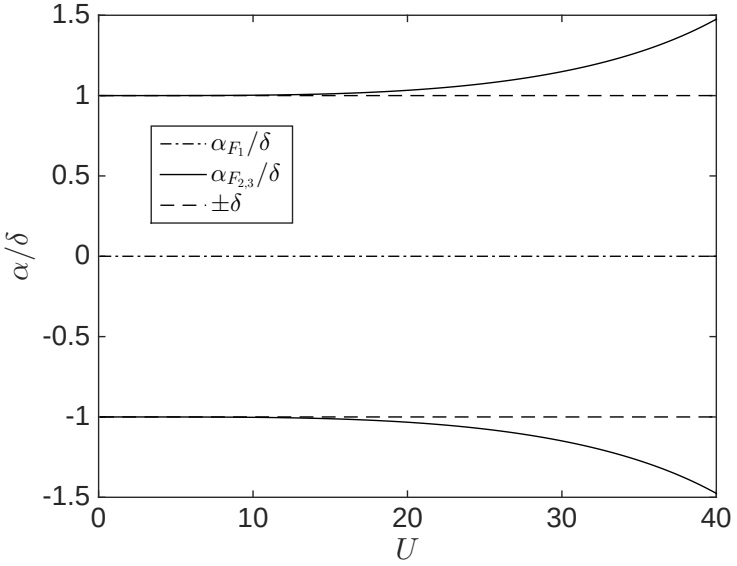


Figure 5: Fixed points of test case system

## 5 TEST CASE

The test case used to demonstrate two-domain limit cycles is the system of equations 2 with the parameter values of the experiment carried out by Conner et al [3] but with freeplay in the pitch degree of freedom instead of the control. The first step is to calculate the resulting system's fixed points using equations 7.

Figure 5 plots the fixed points of the system for different values of the airspeed $U$. It can be seen that points $\mathbf{x}_{F_{2,3}}$ exist at all airspeeds $U > 0$ as they lie outside the freeplay region. At $U = 0$ these points collide with the freeplay boundaries and disappear. This phenomenon is known as a Boundary Equilibirum Bifurcation [9]. Nevertheless, the fact that $\mathbf{x}_{F_{2,3}}$ exist at all other airspeeds means that there is a possibility for two-domain limit cycles.

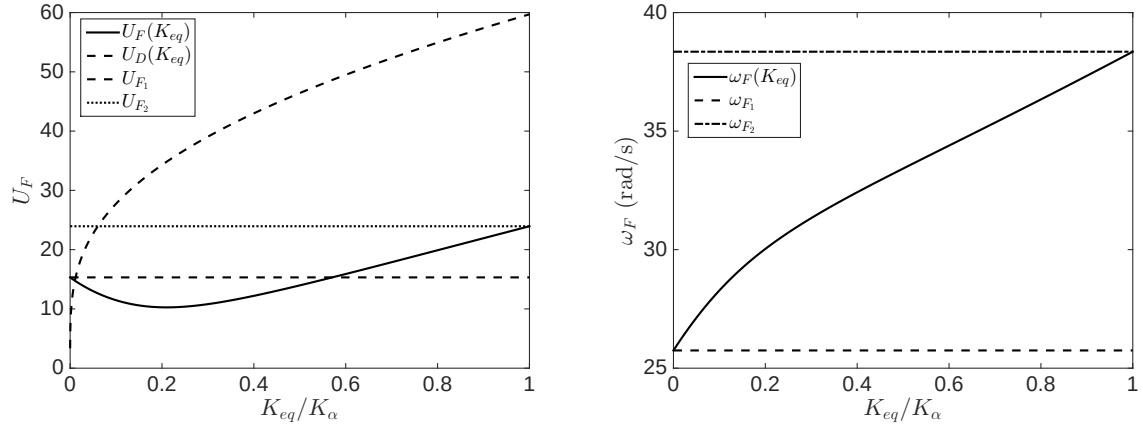


(a) $U_{F_{eq}}$ vs $K_{eq}$

(b) $omega_{F_{eq}}$ vs $K_{eq}$

Figure 6: Flutter speed, frequency and divergence speed for equivalent linearised system.

The stability of the fixed points is as follows:

- $\mathbf{x}_{F_1}$ is a saddle in one eigendirection and a stable focus or node in all the other eigendirections for $U < U_{F_1}$, $U_{F_1} = 15.3$ m/s being the flutter speed of the underlying linear system. For $U > U_{F_1}$ the fixed point is a saddle in one eigendirection, an unstable focis in another and a stable focus or node in all the other directions.
- $\mathbf{x}_{F_{2,3}}$ are stable foci or nodes for $U < U_{F_2}$, $U_{F_2} = 24.0$ m/s being the flutter speed of the overlying linear system. For $U > U_{F_2}$ the fixed points become unstable foci in one eigendirection and remain stable in all the others.

The next step is to calculate the flutter speed $U_{F_{eq}}$, flutter frequency $\omega_{F_{eq}}$ and static divergence speed $U_{D_{eq}}$ for the equivalent linearised system for values of $K_{eq}$ from 0 to $K_\alpha$. Note that the equivalent linearised systems for three-domain limit cycles (equations 11) and for two-domain limit cycles (equations 15) yield the same values of $U_{F_{eq}}$, $\omega_{F_{eq}}$ and $U_{D_{eq}}$ for the same value of $K_{eq}$ since $\mathbf{Q}_{eq}$ is equal for the two systems.

Figure 6(a) plots $U_{F_{eq}}$ and $U_{D_{eq}}$ for $K_{eq}$ from 0 to $K_\alpha$, along with $U_{F_1}$ and $U_{F_2}$. It can be seen that $U_{F_{eq}} = U_{F_1}$ for $K_eq = 0$, as expected, but then it decreases with increasing $K_eq = 0$. It reaches a minimum at around $K_{eq} = 0.2K_\alpha$ and then starts to increase again until $U_{F_{eq}} = U_{F_2}$ for $K_{eq} = K_\alpha$. Figure 6(b) shows that $\omega_{F_{eq}}$ increases monotonically with $K_{eq}$, from $\omega_{F_1}$ the flutter frequency of the underlying linear system to and $\omega_{F_2}$ that of the overlying linear system.

Another interesting aspect of figure 6(a) is that the underlying linear system undergoes static divergence at all airspeeds higher than $U = 0$ m/s. As $K_{eq}$ increases, $U_{D_{eq}}$ increases very quickly and becomes higher than $U_{F_2}$. Note that the pitch-plunge-control wing can undergo static divergence even when the flexural axis lies on or ahead of the aerodynamic centre (in this case it lies on the aerodynamic centre). This phenomenon is due to the aerodynamic stiffness coupling between the pitch and control degrees of freedom.

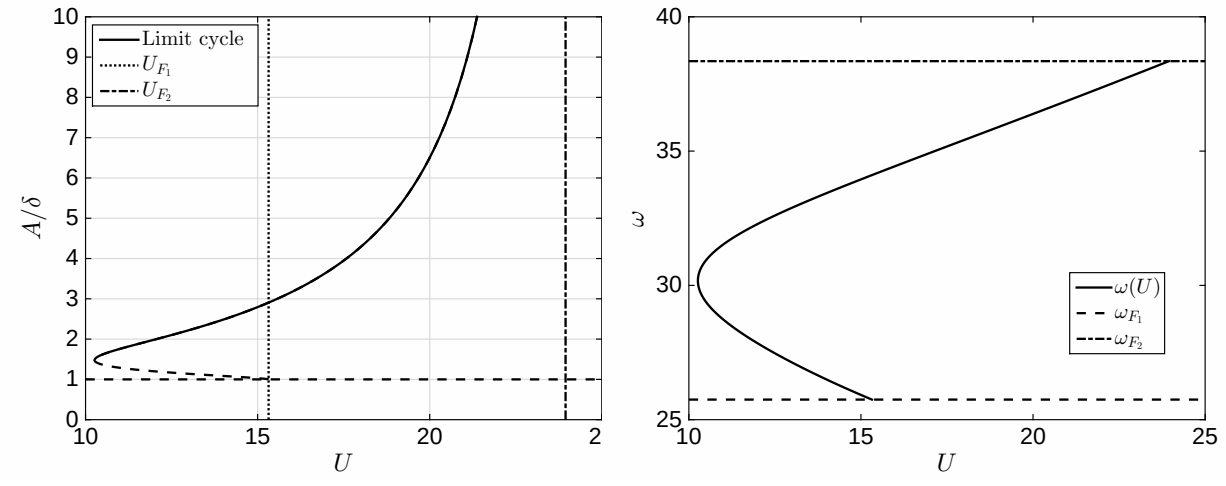


(a) $A$ vs $U$ (b) $\omega$ vs $U$

Figure 7: Limit cycle amplitude and frequency for three-domain cycles.

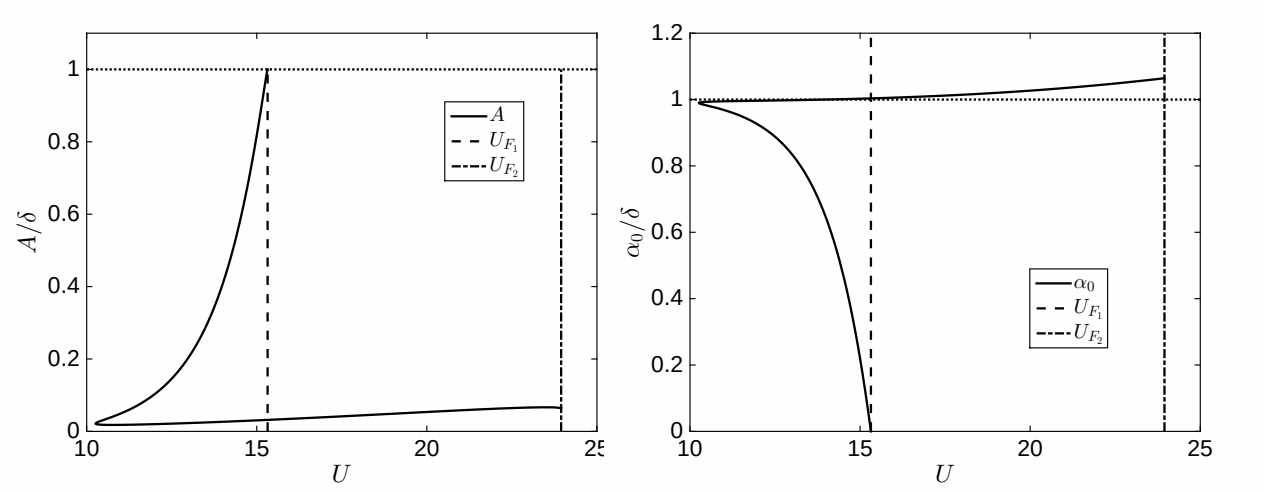


(a) $A$ vs $U$ (b) $\omega$ vs $U$

Figure 8: Limit cycle amplitude and offset for two-domain cycles.

The equivalent stiffness equation 10 for three-domain cycles shows that the $K_{eq}$ is a monotonously increasing function of $A$. Therefore, figure 6(a) can be simply re-plotted after substituting $A$ for $K_{eq}$, resulting in the limit cycle amplitude vs airspeed diagram of figure 7(a). It can be seen that a limit cycle branch appears at $U_{F_1}$ with initial amplitude equal to $\delta$. The limit cycles on it are unstable and increase in amplitude as the airspeed decreases. At an airspeed of just over 10 m/s the branch undergoes a fold bifurcation, becomes stable and starts to increase in amplitude in the increasing airspeed direction. Figure 7(a) clearly shows that, although the nominal system is flutter-free up to an airspeed $U_{F_2} = 24$m/s, the system with freeplay in pitch will undergo three-domain LCOs at airspeeds as low as 10m/s. The frequency of these LCOs starts at 30 rad/s and increases to $\omega_{F_2} = 38.3$ rad/s, the flutter frequency of the overlying linear system, as shown in figure 7(b). The results plotted in figure 7 have already been reported by several researchers investigating typical wing sections with freeplay in pitch. It should also be kept in mind that equivalent linearisation is an approximate solution and that the exact limit cycle branch may be more complex. Nevertheless, figure 7 is an acceptable overview of the bifurcation behaviour as far as three-domain limit cycles are concerned.

The calculation of the two-domain limit cycles starts again with the results of figure 6. Then, the system of equations 16 is solved at each value of $K_eq$ for the corresponding values of $A$ and $\alpha_0$. Figure 8(a) plots the resulting amplitude values. A limit cycle branch appears at $U_{F_1}$ with initial amplitude $A = \delta$, exactly as in the three-domain case. However, $A$ decreases very quickly as the airspeed increases. The branch folds near $U = 10$ m/s, as does the three-domain branch but then the amplitude remains quite small. The branch disappears at $U = U_{F_2}$ when the lower bound of the limit cycle crosses the freeplay boundary. It is clear that the two-domain limit cycles have much smaller amplitude than the three-domain cycle, except at $U = U_{F_1}$ where the two cycles have the same amplitude. The frequency of the two-domain branch is identical to that of the three-domain branch, as plotted in figure 7(b).

Figure 9 plots the two-domain and three-domain limit cycle branches in the $\alpha - \dot{\alpha}$ phase plane against airspeed. Both branches appear at $U_{F_1} = 15.3$ m/s and have amplitude

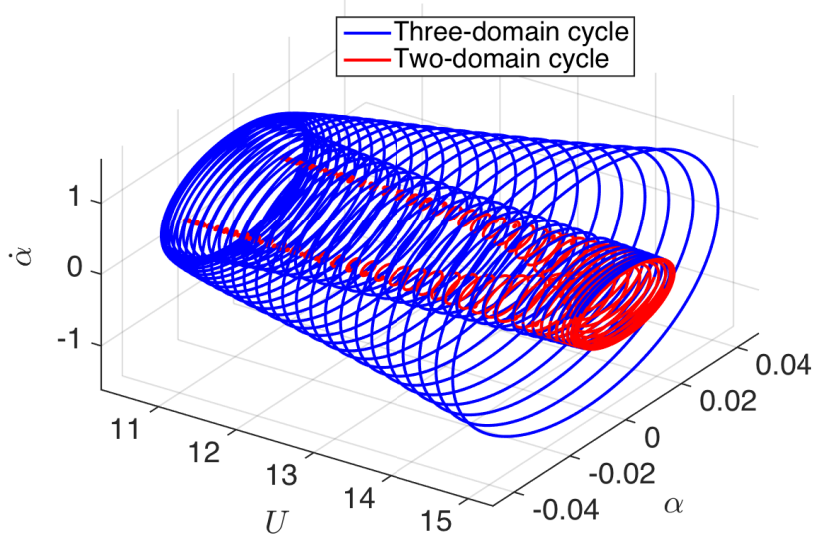


Figure 9: Two-domain and three-domain limit cycles

$A = \delta$. The separate immediately as the airspeed decreases; the three-domain cycle amplitude keeps increases while the the two-domain cycle amplitude decreases. The three-domain cycles are always centred around $\mathbf{x}_{F_1}$ (i.e. the origin) while the two-domain cycles are centred around $\mathbf{x}_{F_{2,3}}$. Nevertheless, both branches fold at the same airspeed $U = 10.3$ m/s. The three-domain cycle becomes stable, while the two-domain cycle becomes unstable.

The bifurcation seen in figure 9 is a grazing bifurcation. The circles that exist in the underlying linear system at $U = U_{F_1}$ intersect with the the freeplay boundary and become limit cycles. The two-domain limit cycles also disappear as a result of a grazing bifurcation; the limit cycle intersects the freeplay boundary and disappear.

## 6 TIME INTEGRATION

The results of the previous section demonstrate that two-domain limit cycles are possible but they are based on equivalent linearization, which is an approximate method. Accurate limit cycles can be calculated using time integration of the equations of motion. In this work, the equations are integrated using a Runge-Kutta-Fehlberg scheme (see for example [10]). The solution methodology includes event detection, i.e. the time instances at which the response trajectory crosses the freeplay boundaries are calculated with high precision.

Figure 10 shows a two-domain limit cycle calculated using time integration from initial conditions $\mathbf{x}_0$. The response trajectory settles onto the cycle after around 4 s. Subfigure 10(b) plots the shape of the limit cycle in the $\alpha - \dot{\alpha}$ phase plane. It can be seen that the cycle does indeed orbit around fixed points $\mathbf{x}_{F_3}$ but it is not a simple ellipse as modelled by equivalent linearisation. In fact, it is a period-2 cycle, which means that the limit cycle branch underwent a period-doubling bifurcation. The limit cycle of figure 10

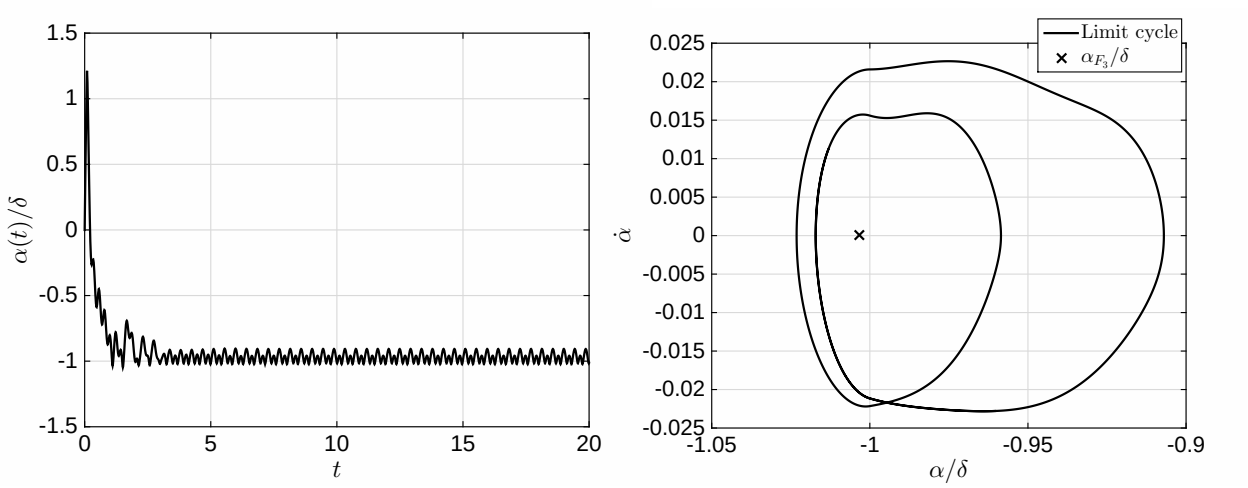


(a) Time domain

(b) Phase plane

Figure 10: Two-domain limit cycle at $U = 11$m/s.

lies in the $S_1$ and $S_3$ subdomains but if the initial conditions are chosen as $-\mathbf{x}_0$ the mirror image cycle will be obtained, which lies in the $S_1$ and $S_2$ subdomains.

Figure 11 plots the shape of the limit cycle in the $\alpha - \dot{\alpha}$ phase plane at four different airspeeds. At $U = 10.5$ m/s, plot 11(a) shows that the limit cycle features only one loop in the phase plane and therefore is period-1. At $U = 11$ m/s (figure 11(b)) the LCO has already bifurcated into a period-2 cycle. At $U = 11.7$ m/s the cycle has further bifurcated to period-4. Finally, at $U = 12$ m/s, it has become completely aperiodic. A period doubling cascade occurs very quickly: period-2 bifurcation at $U = 11.6$ m/s, period-4 at 11.65 m/s and period-8 at 11.75 m/s. Finally, the period-8 limit cycles become aperiodic at 11.8 m/s through a torus bifurcation. The oscillations become chaotic soon afterwards. This combination of period doubling and torus bifurcations leading to chaos has been observed before in aeroelastic systems with freeplay [5].

Figure 9 shows that as the airspeed increases and approaches $U_{F_1} = 15.3$ m/s the two-domain limit cycles increase in amplitude and start to intersect. They eventually join up with the three-period cycle and the circles at $U = U_{F_1}$. This means that the phase plane of the system turns into a triple well potential problem as $U$ increases towards $U_{F_1}$; there are three stable limit cycles that attract the trajectories. The three-domain cycle is much bigger than the other two so there is very little interaction between them. However, a trajectory that orbits one of the two two-domain cycles can also be attracted by the other. It should be recalled that at this airspeed range the two-domain cycles are unstable; the system trajectories are undergoing aperiodic oscillations around the cycles. It is therefore very easy for them to jump from one to the other. This phenomenon can be observed in figure 12 where a response trajectory is plotted against time at $U = 14$ m/s. It can be seen that the response orbits around the $S_1 - S_3$ two-domain cycle for the first 5 s. It then moves to the $S_1 - S_2$ for 10 s, jumps back to the $S_1 - S_3$ cycle for five seconds, up to $S_1 - S_2$ for 20 s, down to $S_1 - S_3$ for 10 s etc. The timing of the jumps is unpredictable and the behaviour is typical of systems characterised by a double well potential.

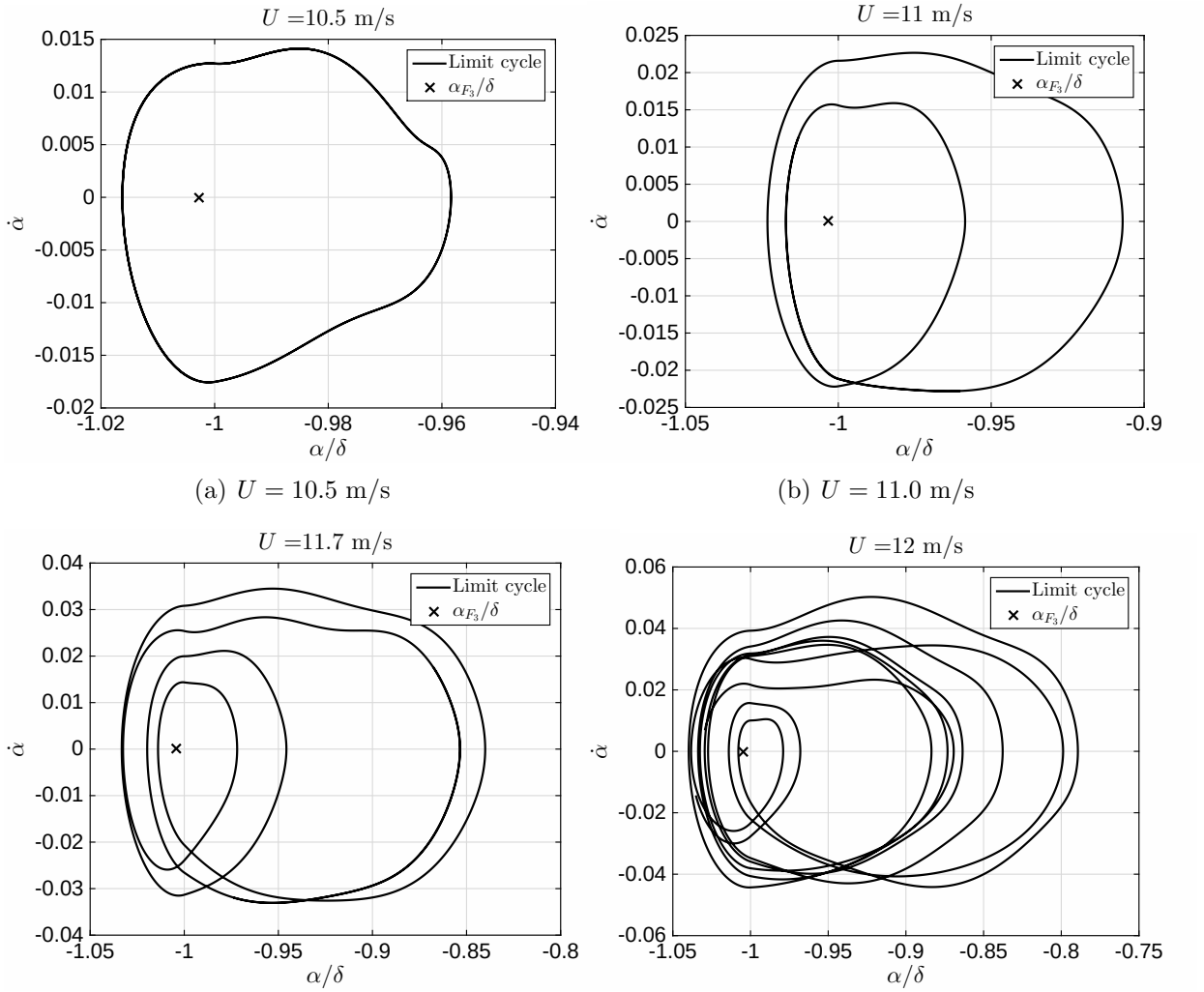


(a) $U = 10.5$ m/s

(b) $U = 11.0$ m/s

(c) $U = 11.7$ m/s

(d) $U = 12.0$ m/s

Figure 11: Two-domain limit cycle shape variation with airspeed.

## 7 CONCLUSIONS

This paper has shown that symmetric aeroelastic system with symmetric freeplay can undergo limit cycle oscillations that do not orbit the origin. These limit cycles are termed two-domain cycles because they span only two of the three piecewise linear subdomains of the system's phase plane. They are generated at the flutter speed of the underlying linear system as the circles of the latter collide with the freeplay boundary. The complete bifurcation is a grazing that leads to three limi cycles, one orbiting the origin (the single three-domain cycle) and two two-domain cycles orbiting anti-symmetric fixed points. In essence, the grazing gives rise to a discontinuous version of the pitchfork bifurcation of cycles. The condition for existence of two-domain limit cycles is that the anti-symmetric fixed points must also exist. The existence of the latter depends uniquely on the nominal linear system and the position of the nonlinearity.

Two-domain limit cycles undergo further bifurcations:

- A fold bifurcation which renders them completely unstable

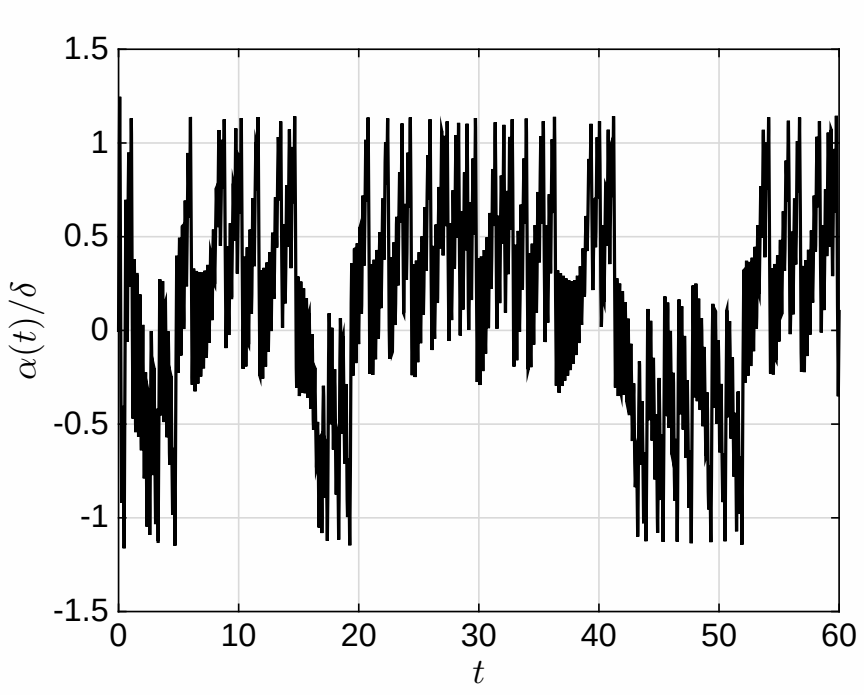


Figure 12: Chaotic limit cycle attracted by both two-domain cycles at $U = 14$ m/s

- A period doubling cascade bifurcation
- A torus bifurcation that causes the oscillations to become aperiodic

Close to the grazing bifurcation point the two antisymmetric two-domain cycles are close enough to each other to interact. Response trajectories are completely chaotic as they are attracted by both the cycles. Moving away from the grazing points, the amplitudes of the two cycles decrease rapidly and the interaction stops. In fact, if either of the two-domain cycle branches is followed away from the grazing point, the period doubling bifurcation is experience as a period-halving cascade.

## 8 REFERENCES

[1] Federal Aviation Administration (2007). Policy for Certification and Continued Airworthiness of Unbalanced and Mass-Balanced Control Surfaces. FAA Policy Memorandum ANM-05-115-019.

[2] Price, S. J., Lee, B. H. K., and Alighanbari, H. (1994). Postinstability behaviour of a two-dimensional airfoil with a structural nonlinearity. *Journal of Aircraft*, 31(6), 1395–1401.

[3] Conner, M. D., Tang, D. M., Dowell, E. H., et al. (1997). Nonlinear behaviour of a typical airfoil section with control surface freeplay: a numerical and experimental study. *Journal of Fluids and Structures*, 11(1), 89–109.

[4] Kholodar, D. B. and Dowell, E. H. (1999). Behavior of airfoil with control surface freeplay for nonzero angles of attack. *AIAA Journal*, 37(5), 651–653.

[5] Dimitriadis, G. (2008). Shooting-based complete bifurcation prediction for aeroelastic systems with freeplay. *Journal of Aircraft*, 48(6), 1864–1877.

[6] di Bernardo, M., Budd, C. J., Champneys, A. R., et al. (2008). Piecewise-smooth dynamical systems: Theory and Applications. Springer.

[7] Yang, Z. C. and Zhao, L. C. (1988). Analysis of limit cycle flutter of an airfoil in incompressible flow. *Journal of Sound and Vibration*, 123(1), 1–13.

[8] Lee, B. H. K., Price, S. J., and Wong, Y. S. (1999). Nonlinear aeroelastic analysis of airfoils: bifurcation and chaos. *Progress in Aerospace Sciences*, 35(3), 205–334.

[9] Di Bernardo, M. and Hogan, S. J. (2010). Discontinuity-induced bifurcations of piecewise smooth dynamical systems. *Philosophical Transactions of the Royal Society*, 368, 4915–4935.

[10] Gerald, C. F. and Wheatley, P. O. (1990). Applied Numerical Analysis. Addison-Wesley, 5th ed.

[11] Theodorsen, T. (1935). General theory of aerodynamic instability and the mechanism of flutter. Tech. Rep. NACA TR-496, NACA.

## 9 APPENDIX

The matrices appearing in equation 3 are given by

$$\mathbf{A} = \begin{pmatrix} m & S & S_\beta \\ S & I_\alpha & I_{\alpha\beta} \\ S_\beta & I_{\alpha\beta} & I_\beta \end{pmatrix}, \quad \mathbf{E} = \begin{pmatrix} K_h & 0 & 0 \\ 0 & K_\alpha & 0 \\ 0 & 0 & K_\beta \end{pmatrix} \tag{17}$$

$$\mathbf{B} = b^2 \begin{pmatrix} \pi & -\pi ab & -T_1 b \\ -\pi ab & \pi b^2(1/8 + a^2) & -(T_7 + (c_h - a)T_1)b^2 \\ T_1 b & 2T_{13}b^2 & -T_3 b^2/\pi \end{pmatrix}$$

where $a = x_f/b - 1$, $b = c/2$, $c_h = x_h/b - 1$, $I_{\alpha\beta} = I_\beta + b(c_h - a)S_\beta$ and the other quantities are given below. The total aerodynamic damping matrix is given by $\mathbf{D} = \mathbf{D}_1 + \Phi(0)\mathbf{D}_2$ where $\Phi(0) = 1 - \Psi_1 - \Psi_2$, $\Phi(t) = 1 - \Psi_1 e^{-\varepsilon_1 U t/b} - \Psi_2 e^{-\varepsilon_2 U t/b}$ is Wagner's function and

$$\mathbf{D}_1 = b^2 \begin{pmatrix} 0 & \pi & -T_4 \\ 0 & \pi(1/2 - a)b & (T_1 - T_8 - (c_h - a)T_4 + T_{11}/2)b \\ 0 & (-2T_9 - T_1 + T_4(a - 1/2))b & bT_{11}/2\pi \end{pmatrix}$$

$$\mathbf{D}_2 = \begin{pmatrix} 2\pi b & 2\pi b^2(1/2 - a) & 2\pi b T_{11}/2\pi \\ -2\pi b^2(a + 1/2) & -2\pi b^3(a + 1/2)(1/2 - a) & -b^3(a + 1/2)T_{11} \\ b^2 T_{12} & b^3 T_{12}(1/2 - a) & b^3 T_{12} b T_{11}/2\pi \end{pmatrix}$$

The total aerodynamic stiffness is given by $\mathbf{F} = \mathbf{F}_1 + \Phi(0)\mathbf{F}_2 + \Xi\mathbf{F}_3$ where $\Xi = \Psi_1\varepsilon_1/b + \Psi_2\varepsilon_2/b$ and

$$\mathbf{F}_1 = b^2 \begin{pmatrix} 0 & 0 & 0 \\ 0 & 0 & (T_4 + T_{10}) \\ 0 & 0 & (T_5 - T_4 T_{10})/\pi \end{pmatrix}$$

$$\mathbf{F}_2 = \begin{pmatrix} 0 & 2\pi b & 2bT_{10} \\ 0 & -2\pi b^2(a+1/2) & -2b^2(a+1/2)T_{10} \\ 0 & b^2T_{12} & b^2T_{12}T_{10}/\pi \end{pmatrix}$$

$$\mathbf{F}_3 = \begin{pmatrix} 2\pi b & 2\pi b^2(1/2-a) & b^2T_{11} \\ -2\pi b^2(a+1/2) & -2\pi b^3(a+1/2)(1/2-a) & -b^3(a+1/2)T11 \\ b^2T_{12} & b^3T_{12}(1/2-a) & b^3T_{12}T_{11}/2\pi \end{pmatrix}$$

The aerodynamic state influence matrix is given by $\mathbf{W} = [2\pi b\mathbf{W}_0 \quad -2\pi b^2(a+1/2)\mathbf{W}_0 \quad b^2T_{12}\mathbf{W}_0]^T$ where

$$\mathbf{W}_0 = \begin{pmatrix} -\Psi_1(\varepsilon_1/b)^2 \\ -\Psi_2(\varepsilon_2/b)^2 \\ \Psi_1\varepsilon_1(1-\varepsilon_1(1/2-a))/b \\ \Psi_2\varepsilon_2(1-\varepsilon_2(1/2-a))/b \\ \Psi_1\varepsilon_1(T_{10}-\varepsilon_1T_{11}/2)/\pi b \\ \Psi_2\varepsilon_2(T_{10}-\varepsilon_2T_{11}/2)/\pi b \end{pmatrix}$$

The $T_1$-$T_{14}$ coefficients are defined in Theodorsen [11] and many other classic aeroelasticity texts. The basic system parameters are:

$$c = 0.254 \text{ m}, \quad s = 0.52 \text{ m}, \quad a = -0.5, \quad c_h = 0.5$$

$$S = 0.08587 \text{ kg m}, \quad S_\beta = 0.00395 \text{ kg m}, \quad I_\alpha = 0.01347 \text{ kg m}^2, \quad I_\beta = 0.0003264 \text{ kg m}^2$$

$$K_h = 2818.8 \text{ kg/m/s}^2, \quad K_\alpha = 37.3 \text{ kg m/s}^2, \quad K_\beta = 3.9 \text{ kg m/s}^2$$

The structural damping parameters are $\zeta_1 = 0.0113$, $\zeta_2 = 0.01626$ and $\zeta_3 = 0.0115$. The structural damping matrix is given by $\mathbf{D} = \mathbf{V}^{-1^T}\mathbf{B}_{mod}\mathbf{V}^{-1}$, where $\mathbf{V}$ are the eigenvectors of the matrix $\mathbf{A}^{-1}\mathbf{E}$ and $\mathbf{B}_{mod}$ is given by

$$\mathbf{B}_{mod} = \begin{pmatrix} 2\bar{m}_1\omega_1\zeta_1 & 0 & 0 \\ 0 & 2\bar{m}_2\omega_2\zeta_2 & 0 \\ 0 & 0 & 2\bar{m}_3\omega_3\zeta_3 \end{pmatrix}$$

In this latest expression, $\bar{m}_i$ are the diagonal elements of the matrix $\mathbf{V}^T\mathbf{A}\mathbf{V}$, $\omega_i$ are the square roots of the eigenvalues of the matrix $\mathbf{A}^{-1}\mathbf{E}$.

## 10 COPYRIGHT STATEMENT